

# Quantum Lithography in Macroscopic Observations

De-Zhong Cao

*Department of Physics, Applied Optics Beijing Area Major Laboratory,  
Beijing Normal University, Beijing 100875, China.*

Kaige Wang\*

*CCAST (World Laboratory), P. O. Box 8730, Beijing 100080, China.  
Department of Physics, Applied Optics Beijing Area Major Laboratory,  
Beijing Normal University, Beijing 100875, China.*

(Dated: October 31, 2018)

We study the generalized Young's double-slit interference for the beam produced in the spontaneously parametric down-conversion (SPDC). We find that the sub-wavelength lithography can occur macroscopically in both the two-photon intensity measurement and the single-photon spatial intensity correlation measurement. We show the visibility and the strength of the interference fringe related to the SPDC interaction. It may provide a strong quantum lithography with a moderate visibility in practical application.

PACS numbers: 42.50.Dv, 42.25.Hz, 42.82.Cr

Young's double-slit interference is a sign of waves, both the classical wave and the quantum de Broglie wave for particles. For a particle, the de Broglie wavelength depends on its mass. When two particles with the same mass combine into a whole, for example, a molecular, the corresponding de Broglie wavelength reduces to the half of that for the single particle. Recently, a similar effect for photons has been investigated both experimentally and theoretically. [1]-[7] Due to the fact of that this effect can overcome the Rayleigh diffraction limit, it may have a prospective application in photon lithography technology. Obviously, the wavelength reduction in Young's interference is a pure quantum phenomenon, and it cannot occur for any classical optical wave. The previous theoretical analysis shows that the quantum lithography effect is based on the optical field in a pure two-photon or multi-photon state. In the experimental observation of the quantum lithography, the detection of single photon pair is carried out by a beam splitter and the two-photon coincidence detection. [2, 4] These studies show that the quantum lithography behaves in a microscopic realm, which limits its practical application because of the weak strength.

The recent investigations show that some quantum effects exhibited in the microscopic observation can also occur in the macroscopic realm. [7, 8] In this paper, we show that the sub-wavelength Young's interference can appear in two macroscopic observations: the two-photon intensity measurement and the single-photon spatial intensity-correlation measurement. The source in the model is the spontaneously parametric down-conversion (SPDC) of a type I crystal. We formulate the second-order correlation function of the field  $G^{(2)}(x_1, x_2) = \langle E^{(-)}(x_1)E^{(-)}(x_2)E^{(+)}(x_2)E^{(+)}(x_1) \rangle$  in the interference plane. In a weak interaction of SPDC when the two-photon state dominates the down-converted beam, the second-order correlation function  $G^{(2)}(x_1, x_2)$  is proportional to the two-photon coincidence probability. But for a strong interaction of SPDC,  $G^{(2)}(x_1, x_2)$  illustrates a macroscopic intensity correlation for a large number of photons. We find that the visibility of the sub-wavelength lithography will not be washed out even in the very strong SPDC process.

The schematic setup of Young's interference is shown in Fig. 1. In observation of two-photon Young's interference, we consider two kinds of measurements: a two-photon detector positioned at  $x$  which scans the two-photon intensity distribution and two single-photon detectors positioned at  $x_1$  and  $x_2$  which measure two-photon coincidence probability or the spatial intensity correlation. We designate  $a_{in}(x, t)$ ,  $a_{out}(x, t)$ ,  $a_1(x, t)$  and  $a_2(x, t)$  the slowly varying field operators in the input plane  $P_{in}$ , the output plane  $P_{out}$  of the crystal, the double-slit plane  $P_1$  and the detection plane  $P_2$ , respectively. The double-slit function  $D(x)$  is defined as

$$D(x) = \begin{cases} 1 & x \in [-\frac{d+b}{2}, -\frac{d-b}{2}] \text{ and } [\frac{d-b}{2}, \frac{d+b}{2}] \\ 0 & \text{others} \end{cases}, \quad (1)$$

where  $b$  and  $d$  are the width of each slit and the interval between two slits, respectively. By ignoring the thickness of the double-slit, the field operator in plane  $P_1$  is obtained as

$$a_1(x, t) = a_{out}(x, t)D(x) + a_{vac}(x, t)[1 - D(x)], \quad (2)$$

---

\*Electronic address: wangkg@bnu.edu.cn

where the vacuum field  $a_{vac}$  is introduced for maintaining the bosonic commutation relation. (Note that  $D^2(x) = D(x)$ .) Since the vacuum field has no contribution to the normal-order correlation, it can be omitted in the calculation. In the paraxial approximation, the transverse field in the detection plane  $P_2$  is written as [9]

$$a_2(x, t) = \frac{1}{2\pi} \iint \tilde{a}_1(q, \Omega) \exp[-i\frac{q^2 z}{2k} + iqx - i\Omega t] dq d\Omega, \quad (3)$$

where  $k$  is the wavenumber of the beam and  $z$  is the distance between the double-slit and the detection plane.  $\tilde{a}_1(q, \Omega)$  is the Fourier transform of  $a_1(x, t)$ . Substituting Eq. (2) into Eq. (3) and considering the integration  $\int_{-\infty}^{\infty} e^{-imq^2 + ixq} dq = (1 - i)\sqrt{\pi/(2m)}e^{ix^2/(4m)}$ , we obtain

$$a_2(x, t) = \frac{1 - i}{2\pi} \sqrt{\frac{k}{2z}} e^{i\frac{kx^2}{2z}} \iint \tilde{a}_{out}(q, \Omega) \mathfrak{D}(q, x) \exp[-i\Omega t] dq d\Omega, \quad (4)$$

where

$$\mathfrak{D}(q, x) = \frac{1}{\sqrt{2\pi}} \int D(x') \exp[i\frac{k}{2z}x'^2 + i(q - \frac{kx}{z})x'] dx'. \quad (5)$$

In the far-field limit  $z \gg kd^2$ , the scale of the interference pattern is much larger than that of the double-slit, Eq. (5) can be approximate to the Fourier transform of the double-slit function  $D(x)$

$$\mathfrak{D}(q, x) \approx \tilde{D}(\frac{kx}{z} - q), \quad (6)$$

where

$$\tilde{D}(q) = \frac{2b}{\sqrt{2\pi}} \text{sinc}(qb/2) \cos(qd/2). \quad (7)$$

Therefore, Eq. (4) can be simplified as

$$a_2(x, t) = \frac{1 - i}{2\pi} \sqrt{\frac{k}{2z}} e^{i\frac{kx^2}{2z}} \iint \tilde{a}_{out}(q, \Omega) \tilde{D}(\frac{kx}{z} - q) \exp[-i\Omega t] dq d\Omega. \quad (8)$$

In the classical regime, we consider a stationary monochromic plane wave in a coherent state  $|\alpha\rangle$ , i.e.  $\langle \tilde{a}_{out}(q, \Omega) \rangle = \alpha \delta(q) \delta(\Omega)$ , which is normally incident upon the double-slit. In the far-field limit, by using Eq. (8), the first-order and the second-order correlation functions for the field in the plane  $P_2$  are respectively obtained as

$$G^{(1)}(x, t) \propto \langle a_2^\dagger(x, t) a_2(x, t) \rangle = \frac{k}{4\pi^2 z} |\alpha|^2 \tilde{D}^2(\frac{kx}{z}), \quad (9)$$

and

$$G^{(2)}(x_1, x_2, t) \propto \langle a_2^\dagger(x_1, t) a_2^\dagger(x_2, t) a_2(x_2, t) a_2(x_1, t) \rangle = \frac{k^2}{16\pi^4 z^2} |\alpha|^4 \tilde{D}^2(\frac{kx_1}{z}) \tilde{D}^2(\frac{kx_2}{z}). \quad (10)$$

Equation (9) gives a single-photon intensity distribution describing a classical Young's interference pattern. However, Eq. (10) illustrates a two-photon Young's interference pattern for  $x_1 = x_2 = x$ , which should be measured by a two-photon detector. These interference patterns have the same interval of fringe-stripe  $\lambda(z/d)$ , showing the same as the classical wave interference.

For an optical parametric amplification (OPA) of the nonlinear crystal of type I, the relationship between the input and the output field is given by [10, 11]

$$\tilde{a}_{out}(q, \Omega) = U(q, \Omega) \tilde{a}_{in}(q, \Omega) + V(q, \Omega) \tilde{a}_{in}^\dagger(-q, -\Omega). \quad (11)$$

The coefficients  $U(q, \Omega)$  and  $V(q, \Omega)$  are written as

$$U(q, \Omega) = \Theta(q, \Omega) \left[ \cosh \Gamma(q, \Omega) + \frac{i\delta(q, \Omega)}{2\Gamma(q, \Omega)} \sinh \Gamma(q, \Omega) \right], \quad (12a)$$

$$V(q, \Omega) = \Theta(q, \Omega) \frac{g}{\Gamma(q, \Omega)} \sinh \Gamma(q, \Omega), \quad (12b)$$

where  $\Gamma(q, \Omega) = \sqrt{g^2 - \delta^2(q, \Omega)/4}$  and  $\Theta(q, \Omega) = \exp\{i[(k_z(q, \Omega) - k)l_c - \delta(q, \Omega)/2]\}$ . The dimensionless mismatch function  $\delta(q, \Omega)$  is given by

$$\delta(q, \Omega) = \delta_0 + \Omega^2/\Omega_0^2 - q^2/q_0^2, \quad (13)$$

where  $q_0 = \sqrt{k/l_c}$  and  $\Omega_0 = 1/(k''_c l_c)$  characterize the spatial-frequency and frequency bandwidths, respectively.  $g$  is the dimensionless coupling strength of the nonlinear interaction and  $\delta_0$  is the phase matching parameter.

Now we consider the model of two-photon double-slit interference for the SPDC interaction shown in Fig. 1. The quantum state of the input field is assumed to be in the vacuum state so that the output field of the crystal is of a SPDC field. Without applying the far field limit, we substitute Eqs. (11) into Eq. (4), and calculate the second-order correlation function of the field  $a_2(x, t)$  in the detection-plane  $P_2$

$$G^{(2)}(x_1, x_2) \propto M(x_1, x_1)M(x_2, x_2) + |M(x_1, x_2)|^2 + |N(x_1, x_2)|^2, \quad (14)$$

where

$$M(x_m, x_n) = \frac{k}{(2\pi)^2 z} \iint |V(q, \Omega)|^2 \mathfrak{D}(q, x_m) \mathfrak{D}^*(q, x_n) dq d\Omega, \quad (m, n = 1, 2) \quad (15a)$$

$$N(x_m, x_n) = \frac{k}{(2\pi)^2 z} \iint V(q, \Omega) U(-q, -\Omega) \mathfrak{D}(q, x_m) \mathfrak{D}(-q, x_n) dq d\Omega. \quad (15b)$$

In order to obtain the analytical form, we consider the broadband limit,  $q_0 \gg 1/d$ . As shown in Ref. [12],  $q_0$  characterizes the spatial-frequency bandwidth of the coefficients  $U(q, \Omega)$  and  $V(q, \Omega)$ . Since the scale of the double-slit function  $D(x)$  is described by the interval  $d$ , the bandwidth of function  $\mathfrak{D}(q, x)$  is characterized by  $1/d$ . The broadband limit can be realized by a thin crystal. In this limit, functions  $U(-q, -\Omega)$  and  $V(q, \Omega)$  are approximately independent of  $q$  in the range where function  $\mathfrak{D}(q, x)$  has significant value and hence are taken as  $U(0, -\Omega)$  and  $V(0, \Omega)$ , respectively. Therefore, we obtain

$$\begin{aligned} M(x_m, x_n) &\approx \frac{k}{(2\pi)^2 z} \iint |V(0, \Omega)|^2 \mathfrak{D}(q, x_m) \mathfrak{D}^*(q, x_n) dq d\Omega \\ &= \frac{k}{(2\pi)^3 z} \iiint |V(0, \Omega)|^2 D(x') D(x'') e^{i\frac{k}{2z}(x'^2 - x''^2) - i\frac{k}{z}(x_m x' - x_n x'') + iq(x' - x'')} dq d\Omega dx' dx'' \\ &= \frac{k}{(2\pi)^2 z} \iint |V(0, \Omega)|^2 D^2(x') e^{-i\frac{k}{z}(x_m - x_n)x'} d\Omega dx' \\ &= f_1 \cdot \tilde{D}\left[\frac{k}{z}(x_m - x_n)\right], \end{aligned} \quad (16a)$$

and similarly,

$$N(x_m, x_n) \approx f_2 \cdot \tilde{D}\left[\frac{k}{z}(x_m + x_n)\right], \quad (16b)$$

where  $f_1 = \frac{k}{(2\pi)^{3/2} z} \int |V(0, \Omega)|^2 d\Omega$  and  $f_2 = \frac{k}{(2\pi)^{3/2} z} \int V(0, \Omega) U(0, -\Omega) d\Omega$ . In Eq. (16),  $D^2(x) = D(x)$  is taken into account. In result, Eq. (14) has the analytical form

$$G^{(2)}(x_1, x_2) \propto |f_2|^2 \left\{ \xi \cdot \tilde{D}^2(0) + \xi \cdot \tilde{D}^2\left[\frac{k}{z}(x_1 - x_2)\right] + \tilde{D}^2\left[\frac{k}{z}(x_1 + x_2)\right] \right\}, \quad (17)$$

where  $\xi = |f_1/f_2|^2$ . Figure 2 shows a 3D plot of  $G^{(2)}(x_1, x_2)$  in the broadband limit.

To show the quantum feature of the second-order correlation of the field in this model, we discuss two kinds of measurements. One of the measurements is so called the two-photon intensity detection in which the detector reacts to a two-photon absorption. When the two-photon detector scans in the plane  $P_2$ , one obtains the distribution  $G^{(2)}(x, x)$ , as shown on the diagonal line  $x_1 = x_2$  of Fig. 2. The other one of the measurements is the spatial intensity correlation, in which two single-photon detectors are placed at positions  $x_1$  and  $x_2$ . For the continuous modes, the field operators at two different positions can commute each other, [10] so that the intensity correlation of two positions is equal to  $G^{(2)}(x_1, x_2)$ , i.e.  $\langle I(x_1)I(x_2) \rangle \propto \langle a^\dagger(x_1)a^\dagger(x_2)a(x_2)a(x_1) \rangle$ . For instance, we set two single-photon detectors at a pair

of symmetric positions  $x_1 = -x_2$  and it measures  $G^{(2)}(x, -x)$  which is shown on the another diagonal line  $x_1 = -x_2$  of Fig. 2. According to Eq. (17), we obtain

$$G^{(2)}(x, x) \propto |f_2|^2 \left\{ 2\xi \cdot \tilde{D}^2(0) + \tilde{D}^2\left[\frac{k}{z}2x\right] \right\}, \quad (18a)$$

$$G^{(2)}(x, -x) \propto |f_2|^2 \left\{ (\xi + 1) \cdot \tilde{D}^2(0) + \xi \cdot \tilde{D}^2\left[\frac{k}{z}2x\right] \right\}. \quad (18b)$$

In comparison with Eqs. (9) and (10), Eqs. (18) show the sub-wavelength interference pattern with a fringe-stripe interval  $(\lambda/2)(z/d)$  for these two measurements. In the previous theoretical treatment, the quantum lithography is explained by the pure two-photon state. However, we show that the quantum lithograph can occur in a general SPDC interaction in which the spontaneous beam contains a large number of photons. Therefore, the measurements of the second-order correlation function can be considered as the macroscopic observations.

The visibilities of the fringes are evaluated as  $\hat{V}_1 = \frac{1}{1+4\xi}$  and  $\hat{V}_2 = \frac{1}{3+2/\xi}$  for  $G^{(2)}(x, x)$  and  $G^{(2)}(x, -x)$ , respectively. Figure 3 shows the visibilities as functions of the parameter  $\xi$ . When  $\xi \ll 1$ , the quantum lithography exists only for the two-photon intensity detection. As  $\xi$  increases,  $\hat{V}_1$  decreases and  $\hat{V}_2$  increases monotonously. In the case  $\xi = 1$ , two kinds of quantum lithography have the same visibility 20%. However, it can be seen that  $\hat{V}_1 > \hat{V}_2$  ( $\hat{V}_1 < \hat{V}_2$ ) when  $\xi < 1$  ( $\xi > 1$ ).

In the practical application of optical lithography, not only the visibility but also the strength of the stripe are important. Nevertheless, the DC background of the interference pattern can be overcome, for example, by coating a covered film on the base. According to Eqs. (18), the strengths of two sub-wavelength fringes described by  $G^{(2)}(x, x)$  and  $G^{(2)}(x, -x)$  are proportional to  $|f_2|^2$  and  $|f_1|^2$ , respectively. In Fig. 4, we plot  $|f_i|^2$  ( $i = 1, 2$ ) and  $\xi$  as functions of the coupling strength  $g$  for the different phase matching  $\delta_0$ . For a weak SPDC process,  $g \ll 1$ ,  $\xi$  and  $|f_2|^2$  are also small. It shows a weak sub-wavelength fringe with the better visibility only for the two-photon intensity detection. This corresponds to the case in which the pure two-photon state dominates the SPDC beam. As  $g$  is increased,  $\xi$  and  $|f_i|^2$  are increased, too. Consequently, the visibility  $\hat{V}_1$  diminishes but  $\hat{V}_2$  enhances. However, for the very strong SPDC interaction,  $g \gg 1$ ,  $\xi$  tends toward about 1 and  $|f_i|^2$  keeps exponentially increasing. According to Fig. 3, two visibilities reach 20% while the strength of the sub-wavelength lithograph can be enhanced greatly. Both Figs. 3 and 4 are helpful to choose the operation of crystal for the optimum lithography application. As some examples, by setting different phase matching parameters  $\delta_0$ , we plot several sub-wavelength interference patterns in Figs. 5, in which Figs. 5a-5c and Figs. 5d-5f show  $G^{(2)}(x, x)$  for the two-photon intensity detection and  $G^{(2)}(x, -x)$  for spatial intensity-correlation detection, respectively. The coupling strength  $g = 1$  given in Fig. 5 indicates the maximum amplification factor  $\exp(2g) \approx 7.4$  in the optical parametric amplifier. [11]

In summary, we formulate the second-order correlation in a double-slit interference for the SPDC beam in the broadband limit. We show that the sub-wavelength interference can occur in a general SPDC process, both the weak and the strong interactions. The quantum lithography can be considered as macroscopic observation since it can occur for a general SPDC process. The two kinds of observations, the two-photon intensity detection and the single-photon spatial intensity correlation detection, provide alternative method. Moreover, the intensive interference beam makes quantum lithography technology in practicability.

### Acknowledgments

This research is funded by the National Fundamental Research Program of China with No. 2001CB309310, and the National Natural Science Foundation of China, Project Nos. 60278021 and 10074008.

- 
- [1] J. Jacobson, G. Björk, I. Chuang and Y. Yamamoto, Phys. Rev. Lett. 74, (1995) 4835.
  - [2] E. J. S. Fonseca, C. H. Monken and S. Pödua, Phys. Rev. Lett. 82, (1999) 2868.
  - [3] A. N. Boto, P. Kok, D. S. Abrams, S. L. Braunstein, C. P. Williams and J. P. Dowling, Phys. Rev. Lett. 85, (2000) 2733.
  - [4] M. D'Angelo, M. V. Chekhova and Y. H. Shih, Phys. Rev. Lett. 87, (2001) 013602.
  - [5] G. Björk, L. L. Sanchez-Soto and J. Soderholm, Phys. Rev. Lett. 86, (2001) 4516; Phys. Rev. A 64, (2001) 013811.
  - [6] P. Kok and et al, Phys. Rev. A 63, (2001) 063407.
  - [7] E. M. Nagasako, S. J. Bentley, R. W. Boyd and G. S. Agarwa, Phys. Rev. A, 64, (2001) 043802.
  - [8] A. Gatti, E. Brambilla and L. A. Lugiato, Phys. Rev. Lett. 90, (2003) 133603.

- [9] L. Mandel and E. Wolf, Optical Coherence and Quantum Optics, Cambridge University Press, Cambridge (1995).  
 [10] M. I. Kolobov and L. A. Lugiato, Phys. Rev. A 52, (1995) 4930.  
 [11] I. V. Sokolov, M. I. Kolobov and L. A. Lugiato, Phys. Rev. A 60, (1999) 2420.  
 [12] K. Wang, G. Yang, A. Gatti and L. A. Lugiato, J. Opt. B: Quantum Semiclass. Opt. 5, (2003) S1.

captions for figures

Figure 1 Schematic setup of the Young's double-slit interference for the SPDC process.

Figure 2 3-D plot of the second-order correlation function  $G(X_1, X_2)$  in which  $X_i = \frac{kb}{2\pi z}x_i$  ( $i = 1, 2$ ) is the normalized position. We set  $\delta_0 = 0$ ,  $g = 1.84$ , and  $d = 5b$ .

Figure 3 Visibilities as functions of the parameter  $\xi$  for two kinds of measurements.

Figure 4 Parameters  $\xi$  and  $|f_2|^2$  as functions of the coupling strength  $g$  for different phase matchings  $\delta_0$ .

Figure 5 Sub-wavelength interference fringes: (a)-(c) for  $G^{(2)}(x, x)$  and (d)-(f)  $G^{(2)}(x, -x)$ .

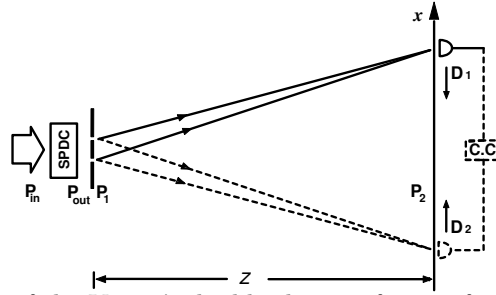


Figure 1 Schematic setup of the Young's double-slit interference for the SPDC process.

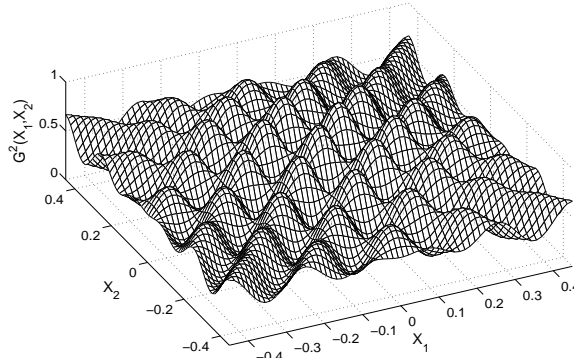


Figure 2 3-D plot of the second-order correlation function  $G(X_1, X_2)$  in which  $X_i = \frac{kb}{2\pi z}x_i$  ( $i = 1, 2$ ) is the normalized position. We set  $\delta_0 = 0$ ,  $g = 1.84$ , and  $d = 5b$ .

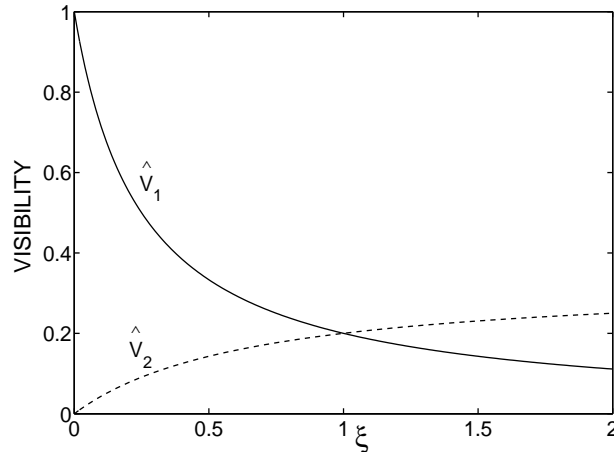
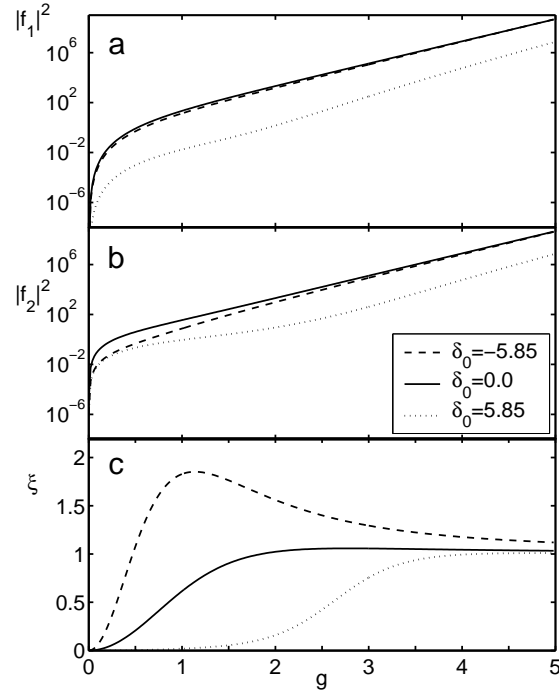
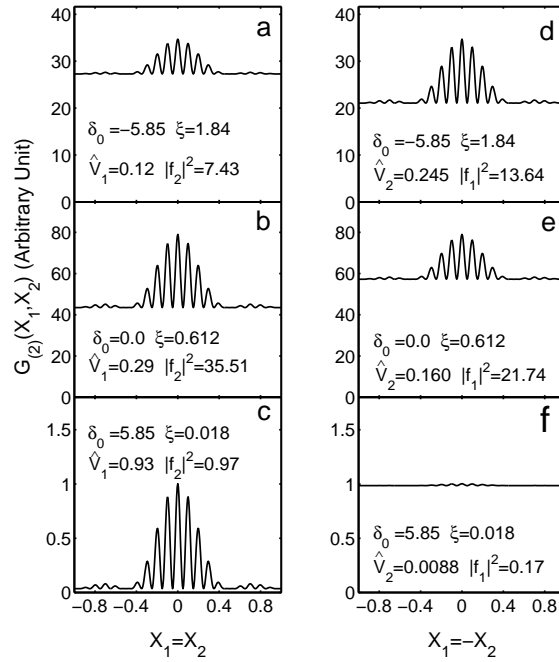


Figure 3 Visibility

of measurements.

Figure 4 Parameters  $\xi$  and  $|f_2|^2$  as functions of the coupling strength  $g$  for different phase matchings  $\delta_0$ .Figure 5 Sub-wavelength interference fringes: (a)-(c) for  $G^{(2)}(x, x)$  and (d)-(f)  $G^{(2)}(x, -x)$ .